Persistent vibrational spectral hole burning and dephasing properties of orientationally aligned CN^- defects in cesium halide crystals

M. Schrempel, W. Gellermann, and F. Luty
Physics Department, University of Utah, Salt Lake City, Utah 84112
(Received 5 September 1991)

Persistent spectral hole burning was used to study the dephasing mechanism of vibrationally excited K^+:CN^- pair defects in cesium chloride crystals. The K^+:CN^- pair defects are formed by statistical association of CN^- and K^+ doping impurities. They occur in two nonequivalent oppositely oriented ⟨111⟩ configurations (CN^-:K^+ or NC^-:K^+) with corresponding spectrally separated transitions. Continuous optical excitation of either configuration in its second-harmonic transition (near 4000 cm^{-1}) with a narrow-linewidth color-center laser leads to 180° CN^- flips in spectrally selected K^+:CN^- defects. This produces, with efficiencies in the 10^{-5} range, a spectral hole in the laser-excited transition and a corresponding (slightly broadened) antihole in the other transition. The spectral holes were burned, and both the holes and antiholes were probed with the same single-mode-tunable color-center laser. Measurements of the holewidth under variation of defect concentration and crystal temperature reveal that the excited-state dephasing of the K^+:CN^- pair defects is strongly influenced by the motional behavior (tunneling, hindered rotation) of the isolated, i.e., not K^+-associated, CN^- molecules. The low-temperature ($T=5$ K) residual holewidth (as low as 20 MHz) is attributed to an elastic dipole-dipole interaction between the excited K^+:CN^- defect and the isolated CN^- molecules. We discuss this mechanism in an elastic-continuum model where the isolated CN^- molecules, which tunnel rapidly at this temperature between their eight ⟨111⟩ equilibrium orientations, are the source of fluctuating strain fields in the crystal and cause "dynamic strain broadening." The holewidth varies linearly with the concentration of the isolated CN^- molecules, in agreement with the model. Under temperature increase the homogeneous linewidth broadens with a T^2 dependence up to the ~40 K thermal-stability limit of the spectral holes. This T^2 behavior far below the Debye temperature ($T_D=165$ K for CsCl) indicates a non-Debye effective phonon density of states with a large number of low-frequency modes participating in the dephasing of the K^+:CN^- defects. In fact, the experimental data are consistent with theory for Raman scattering of phonons peaking in their density of states in the 10-cm^{-1} range. Candidates for this excitation are hindered-rotor levels of isolated CN^- molecules or possibly an internal low-frequency mode of the K^+:CN^- defect itself.

I. INTRODUCTION

Persistent spectral hole burning[1] in inhomogeneously broadened (electronic or vibrational) transitions of defects in solids is widely used as a high-resolution technique to measure the intrinsic homogeneous linewidth of the transition and thus to determine the excited-state dephasing time T_2. If combined with measurements of the excited state lifetime T_1 this technique permits us to study the dynamics of the excited state and to obtain information about its interaction with crystal phonons, defect modes, or other excitations. In addition, narrow persistent spectral holes can be used as sensitive probes for external perturbations of the systems. Previous applications of persistent spectral hole burning have mostly included *electronic* excitations of impurities in the visible region—largely due to the commercial availability of suitable laser sources in that range. In comparison, pure *vibrational* excitations of molecules in solids in the infrared have received rather little attention.[2–5]

In this paper we describe hole burning and excited-state dephasing properties of orientationally aligned CN^- molecular defects in cesium halide crystals. CN^- molecules associated with (and aligned by) F centers in these hosts have recently gained importance as strong solid-state ir vibrational emitters[6–8] and stable laser active materials.[9]

II. BACKGROUND

Isolated CN^- molecules in alkali halide matrices perform reorientational motions on their lattice sites at practically all crystal temperatures, evolving from tunneling at lowest temperatures over libration and hindered rotation to quasifree rotation at high temperatures ($T \geq 30$–120 K depending on the host).[10,11] They become orientationally aligned if associated with a neighboring alkali cation impurity (M^+), thus forming a M^+:CN^- pair defect. Spectroscopic investigations of such defect systems have included Li^+-, Na^+-, and Rb^+-aligned CN^- in KBr,[4] and K^+- and Rb^+-aligned CN^- in cesium halide hosts.[12]

An ionic model of a CN^- defect aligned by a K^+ ion in a cesium halide crystal is shown in Fig. 1 together with a model for an unpaired (isolated) CN^- molecule in the same host.[12] The isolated CN^- molecule is a substitu-

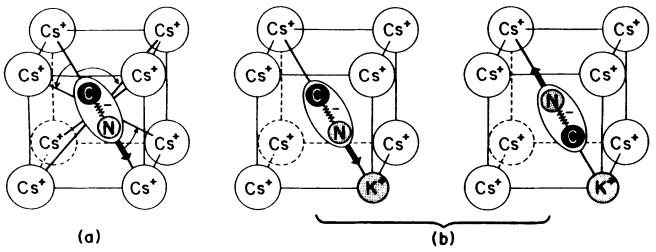

FIG. 1. Schematic illustration of ionic structure of CN^- defects in cesium halides. (a) Isolated CN^- defect: weakly hindered rotor between eight equivalent ⟨111⟩ orientations; (b) CN^- defect aligned in two opposite ⟨111⟩ electric dipole orientations by neighboring K^+ impurity.

tional defect on a halide site; it performs weakly hindered reorientations between eight equivalent ⟨111⟩ directions. The orientationally aligned K^+:CN^- defect pair consists of a CN^- molecule on a halide site and a K^+ ion nearest neighbor in a ⟨111⟩ direction. Depending on whether the N or the C end of the CN^- electric dipole (~0.6 Debye) faces the K^+ ion, two molecular configurations exist, CN^-:K^+ and NC^-:K^+, with slightly different vibrational eigenfrequencies. Figure 2 shows the absorption spectra of a CsCl crystal, containing K^+:CN^- pair defects, in the temperature range 20–300 K. The crystal is doped with 0.5% KCN and 0.5% KCl and contains $\sim 1\times10^{-2}$ mol parts K^+, 3×10^{-3} isolated CN^-, and 1×10^{-3}

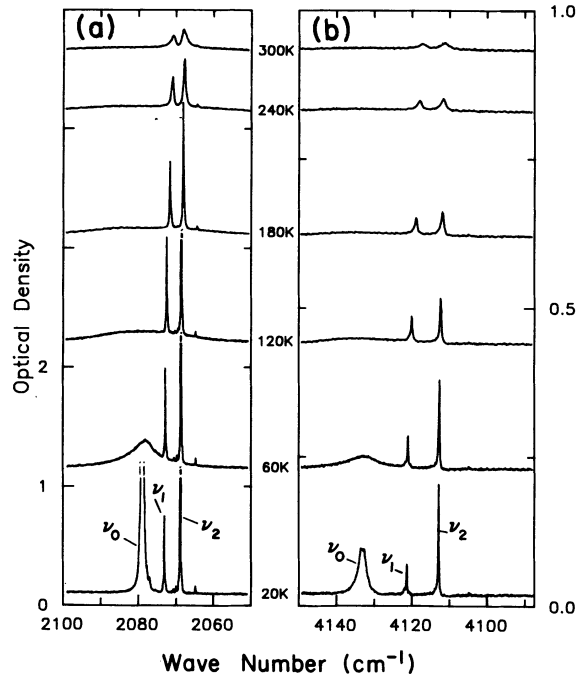

FIG. 2. Fundamental (a) and second harmonic (b) CN^- vibrational absorption spectra, measured between 20 and 300 K in CsCl, containing $\sim 1\times10^{-2}$ mol parts K^+, 3×10^{-3} CN^-, and 1×10^{-3} K^+:CN^-; sample thicknesses were 0.65 mm (a) and 8.5 mm (b). Note scale change of optical densities for fundamental and second harmonic transitions.

K^+:CN^- pair defects. In the absorption spectra, shown for the fundamental and second harmonic CN^- vibrational transitions, the K^+:CN^- transitions (ν_1 and ν_2) appear as low-energy satellite peaks of the isolated CN^- transition (ν_0). With increasing crystal temperatures the K^+:CN^- transitions remain sharp—due to their rotational alignment—whereas the isolated CN^- transition broadens into the unresolved spectrum of a quasifree rotor.[12]

The orientationally aligned K^+:CN^- defects are produced during crystal growth by statistical association of CN^- with K^+ impurities. As a consequence, isolated K^+ and CN^- impurities are present in the crystal in much higher concentrations (typically 1–2 orders of magnitude) than the K^+:CN^- pair defects. If n_{K^+} and n_{CN^-} are the impurity concentrations in the crystal, the statistically expected K^+:CN^- pair concentration is $8n_{K^+}n_{CN^-}$, where eight is the coordination number in the bcc lattice structure.

Spitzer *et al.*[4] investigated the usefulness of Li^+-, Na^+-, and Rb^+ associated CN^- molecules in KBr for persistent spectral hole burning. Using diode laser excitation of the fundamental transitions of the defects near 5 μm they showed that narrow persistent spectral holes can be produced in the vibrational transitions of one system (Na^+:CN^-) but not in the others (Li^+:CN^- or Rb^+:CN^-). The underlying hole burning mechanism was proposed to be a 180° flip of the CN^- molecule between the two inequivalent Na^+:CN^- energy configurations, occurring during vibrational deexcitation. Since this mechanism was not seen to be effective in all investigated systems, open questions remain concerning the underlying physical processes.

Recently it was shown that K^+ as well as Rb^+ aligned CN^- defects are suitable for persistent spectral hole burning and antihole production in the bcc hosts CsCl, CsBr, and CsI.[13] The holes were produced with burning efficiencies in the range from 10^{-4} to 10^{-8} and were as narrow as 20 MHz (7×10^{-4} cm^{-1}). Depending on the host and the stabilizing impurity the spectral holes were persistent up to $T=40$ K. This situation allows one to study persistent hole burning effects for a whole class of defects in this temperature range under variation of both host and impurity parameters.

In this paper we describe a systematic study of persistent holes produced in the second harmonic vibrational transitions of K^+:CN^- defects in CsCl, and their dependence on defect concentrations and crystal temperature. Due to the long spontaneous lifetime of these transitions (ms range) their natural linewidth is expected in the kHz range. The measured homogeneous linewidths, however, as deduced from the widths of the persistent spectral holes, are seen to be several orders of magnitude larger and thus show the existence of some fast dephasing mechanisms.[13] The subject of this paper is to identify the nature of these dephasing mechanisms.

The remainder of this paper is structured as follows. The experimental techniques are described in Sec. III. Section IV contains experimental results on thermal hole decay and on the dependence of the holewidths on crystal

temperature and impurity concentrations. In Sec. V the results are discussed. A temperature independent contribution to the dephasing of K^+:CN^- defects is argued to occur via interaction with the fluctuating strain fields produced by isolated CN^- molecules; this mechanism is treated within the framework of an elastic dipole model. The observed variation of the homogeneous linewidth with temperature is compared with various theoretical models for dephasing by phonons and is shown to be consistent with Raman scattering of a low-energy (~ 10 cm^{-1}) excitation.

III. EXPERIMENTAL TECHNIQUES

Cesium halide crystals, double-doped with alkali cations and CN^- molecules, were grown from the melt in the Utah Crystal Growth Lab using standard Czochralski techniques. Doping materials were KCl and CsCN (or KCN, when a fixed $[K^+]/[CN^-]$ ratio was desired) for K^+:CN^- systems, and RbCl and RbCN for Rb^+:CN^- systems. The K^+ doping was varied between 1×10^{-4} and 2×10^{-2} mol (the solubility limit), and the CN^- concentration between 1×10^{-4} and 5×10^{-3} mol.

Concentrations of isolated CN^- molecules in the boules were obtained from the absorption strength S [integrated absorption coefficient $\alpha(\nu)$] of the fundamental ν_0 transition at room temperature using the known correlation $S/n_{CN^-}=2.9\times10^{-18}$ cm for CsCl, $S/n_{CN^-}=2.4\times10^{-18}$ cm for CsBr, and $S/n_{CN^-}=2.0\times10^{-18}$ cm for CsI.[14] The spectra were measured with a commercial FTIR spectrometer (Bruker Instruments IFS 88) having a spectral resolution of 0.11 cm^{-1}. Concentrations of the K^+:CN^- pair defects were obtained in the same way assuming the same oscillator strength for the K^+:CN^- ν_1 and ν_2 transitions as for the ν_0 transition of the isolated CN^- molecule. For low K^+:CN^- concentrations, where the ν_1 and ν_2 lines were too weak (at room temperature) and too narrow (at low temperatures) to be accurately measured with the FTIR, the line strength S was measured with a higher-resolution laser spectrometer (see below) in the second harmonic absorption at helium temperatures. The K^+:CN^- concentrations were found to vary between 7.5×10^{-7} and 1.1×10^{-3}, and the isolated CN^- concentration between 2.5×10^{-5} and 3.2×10^{-3}. Compared to the statistically expected K^+:CN^- concentration ($8n_{K^+}n_{CN^-}$) the actual concentration in the samples was found to be higher by a factor of 5–6 in low doped crystals while in higher doped ones it was close to the expected level.

A block diagram of the experimental setup is provided in Fig. 3. To burn spectral holes and measure their spectral profile with high resolution, a computed-controlled laser spectrometer was designed and set up, based on a commercial color-center laser (Burleigh FCL-20). The laser is used to both burn spectral holes and, with a much reduced intensity, to probe their spectral profiles. Laser tuning is realized with a personal computer which is interfaced to the tuning elements of the resonator.[15] Spectra are recorded using a dual beam arrangement: while the laser frequency is tuned across the spectral region of interest, the transmitted light intensity through the sample is detected together with the light intensity before the sample. The sample transmission data for each wavelength increment are calculated and stored by the computer, thus allowing digital processing of the data.

The laser crystal is a KCl:Li F_A(II) center crystal with a tuning range of $\sim$2.4–2.9 μm. This covers the second harmonic of the vibrational transitions of CN^- molecules in all host lattices. The laser had to operate on a single longitudinal cavity mode for maximum spectral resolution.

For survey scans of an absorption line the laser frequency could be tuned in discrete steps (cavity mode sep-

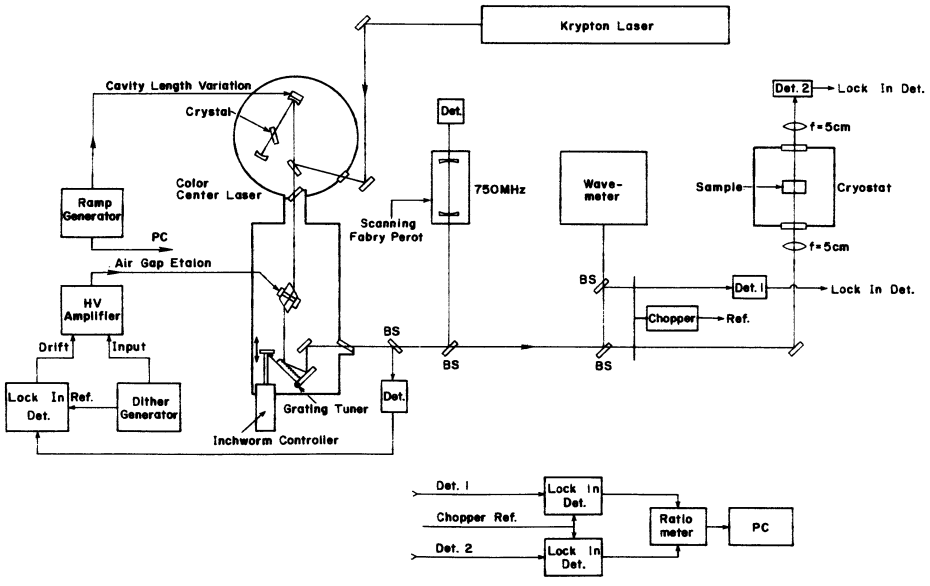

FIG. 3. Experimental setup (see text).

aration of 300 MHz=0.01 cm^{-1}) over a range of 45 GHz (1.5 cm^{-1}). This was done by varying the air gap of the intracavity étalon. To measure spectral features with the full resolution of the laser linewidth, the laser could also be tuned continuously over a reduced spectral range of ~2.5 GHz (~0.08 cm^{-1}). This was done by a computer-controlled piezoelectric extension of the cavity length while the air gap étalon was locked onto the cavity mode by an active feedback loop[16] to prevent "mode hopping."

The spectral resolution of the laser spectrometer (given by the laser linewidth) was measured to be better than 20 MHz (~6.5×10^{-4} cm^{-1}). This spectral linewidth proved to be sufficiently narrow for our experiments and there was no need to set up a complicated active frequency stabilization technique, which would have to be based on a stable external frequency reference.

The absolute laser frequency was monitored by a wavemeter (Burleigh WA-20) with a resolution of 0.01 cm^{-1}. A relative frequency reference was added using a confocal scanning Fabry-Perot interferometer with a free spectral range of 750 MHz (0.025 cm^{-1}) and a finesse of ~40. For a particular scan, the laser frequency starting and end points were correlated to the interferometer, and each intermediate data point was determined through linear interpolation, assuming a linear response of the laser tuning elements to the control signals. The actuators used in the laser system were piezoceramics with known nonlinearities at the extremes of their extension ranges. These regions were avoided.

The sample was mounted onto a copper cold finger in a liquid helium cryostat. Thermal contact of the crystal holder with the helium reservoir was made either by direct contact or by helium exchange gas, the latter option permitting a variation of the sample temperature with a heater. With the exchange gas setup the sample temperature could be varied between ~5 K and liquid nitrogen temperature. A temperature readout was provided by a silicon diode (Lake Shore DT-500-DRC-D) with a specified accuracy of ±0.5 K and a repeatability of 50 mK. With an excitation current of 10 μA the sensor dissipated only ~20 μW into the sample assembly. The heater was controlled by a cryogenic temperature controller (Lake Shore DTC-500) which could keep temperatures constant to within ±0.2 K.

The laser beam was focused onto the sample by a $f=45$ mm lens. The laser beam radius in front of the focusing lens was found to vary between 0.64 and 0.72 mm when the frequency was tuned through the maximum continuous scan range. With an approximate value of 0.7 mm for the beam radius the diffraction limited laser spot size in the sample is calculated as 8×10^{-5} cm^2. A typical single-mode laser output power of 3 mW then results in an intensity in the focused spot of 30 W/cm^2. For recording spectral profiles the intensity could be attenuated by a factor of 500–1000 to give a probing intensity of 30–60 mW/cm^2. This intensity level did not produce any detectable persistent changes in absorption before and after a scan. The transmitted light was then refocused onto a PbS detector operating at room temperature. An identical detector was used to record the laser light level before the sample. The laser light was modulated by a mechanical chopper with a frequency of ~200 Hz. The ac signal of the detectors were amplified by two identical Lock-In amplifiers (Stanford Applied Research SR 510), and their outputs were sampled by the computer for the calculation of the sample transmission. The main source of noise in the recorded spectra was found in the intensity fluctuations of the laser. While the effect of these fluctuations should be largely eliminated by the dual beam arrangement of the setup, slightly different responses of sample and reference arm pose a limiting factor. Under optimum conditions the minimal detectable change in transmission was ~0.04%, corresponding to a change in optical density of ~2×10^{-4}.

IV. EXPERIMENTAL RESULTS

A. Spectral holes and antiholes

Persistent spectral hole burning could be obtained in the second harmonic vibrational ν_1 and ν_2 transitions of both K^+:CN^- and Rb^+:CN^- defects in CsCl, CsBr, and CsI host crystals with hole burning efficiencies in the 10^{-5} to 10^{-4} range. The Rb^+:CN^- defect in CsI is an exception since it has a smaller hole burning efficiency (10^{-8} to 10^{-7} range) and shows a hole decay with a half-lifetime of ~$\frac{1}{2}$ h at liquid helium temperature. The burning of a spectral hole (up to 100% deep) in one transition is in all cases accompanied by the formation of a corresponding antihole in the other transition. This is shown in Fig. 4 for K^+:CN^- defects in CsCl. The particular sample contained a K^+:CN^- defect pair concentration of ~8.3×10^{-6}, a K^+ concentration ~1×10^{-3}, and an isolated CN^- molecule concentration of ~3.2×10^{-4}.

The antihole area in the ν_1 transition is 85%±20% of the corresponding hole area in the ν_2 transition indicating a slightly decreased oscillator strength for the ν_1 transition. The hole formation process is optically reversible: hole burning in the ν_1 transition leads with the same hole burning efficiency, thermal stability, and spectral holewidth to the formation of an antihole in the ν_2 transition. Since the antihole is broader than the corresponding hole (by a factor of about 3), it is possible to burn a spectral hole into the antihole. Spectral hole burning experiments with an oriented sample showed that the defect pairs are aligned along the ⟨111⟩ directions in the crystal and that a spectral hole and the corresponding antihole have the same polarization.[13] These results indicate clearly that the underlying mechanism for the hole formation is an optically induced 180° reorientation of the CN^- molecule in vibrationally excited K^+:CN^- or Rb^+:CN^- defect pairs.

B. Thermal hole decay

Figure 5(a) shows the thermal stability of a hole burned into the ν_2 transition of K^+:CN^- defects in CsCl, CsBr, and CsI hosts. For these measurements a deep hole was burned at $T=5$ K, the sample heated to a higher temperature, and the relative hole depth measured after keeping

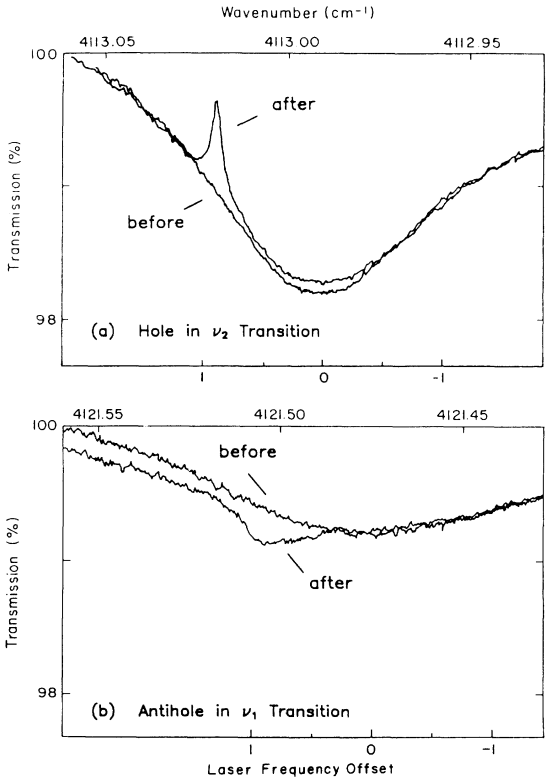

FIG. 4. Persistent spectral hole burning in ν_2 vibrational transition (a) and simultaneous antihole production in ν_1 vibrational transition (b) of K^+:CN^- defects in CsCl, containing $\sim 1\times10^{-3}$ K^+, 3.2×10^{-4} CN^-, and 8.3×10^{-6} K^+:CN^-. The apparent extension of the spectral antihole toward higher wave numbers is an experimental artifact.

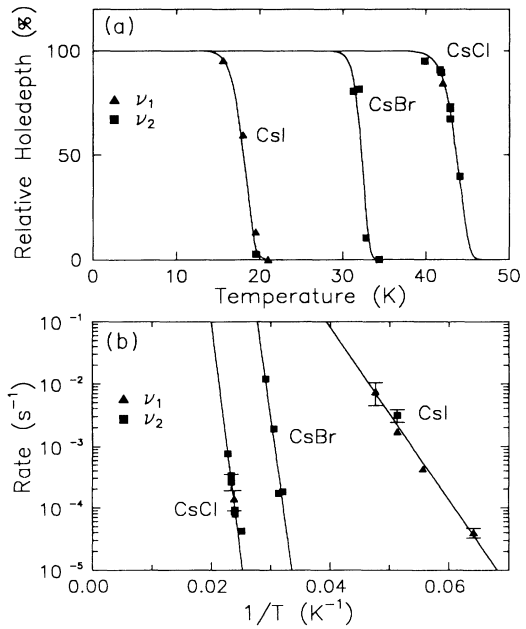

FIG. 5. Thermal stability of spectral holes burned into the ν_2 transition of K^+:CN^- defects in cesium halides. (a) Relative change in hole depth after heating to indicated temperatures for 20-min-observation time. (b) Hole-decay rates τ vs $1/T$. The solid lines are Arrhenius fits $1/\tau=\nu_0\exp(-U_0/kT)$ to the data points.

the samples at that specific temperature for 20 min. This procedure was repeated for a series of stepwise increased temperatures. Depending on the host, the holes are stable up to a specific critical temperature above which they rapidly decay in an almost stepwise fashion. For the K^+:CN^-/CsCl system it was seen that the thermal hole stability is independent of the K^+:CN^- concentration. The critical temperatures are $T\approx40$ K for CsCl, $T\approx30$ K for CsBr, and $T\approx15$ K for CsI, thus decreasing in the order of increasing lattice constants. The critical temperatures for Rb^+:CN^- defects, measured in an analogous way, were found to be lower compared to their K^+:CN^- counterparts in the same host: $T\approx25$ K for CsCl, $T\approx5$–10 K for CsBr, while for a CsI host the holes are unstable even at $T=4.2$ K.

For K^+:CN^- defects the behavior of the holes in the temperature range of thermal instability was investigated in greater detail. When monitoring the hole depth as a function of time it was seen that the hole decays with an $\exp(-t/\tau)$ dependence in all hosts. The rates $1/\tau$ are plotted versus inverse temperature in Fig. 5(b) for all three hosts. They can be fitted to an Arrhenius law $1/\tau=\nu_0\exp(-U_0/kT)$ with activation energies $U_0=1750\pm90$ K for CsCl, $U_0=1500\pm900$ K for CsBr, and $U_0=320\pm25$ K for CsI. The attempt frequency ν_0 for CsCl and CsBr hosts ν_0 ranges between 10^{13} and 10^{15} s^{-1}; for a CsI host ν_0 lies between 2×10^4 s^{-1} and 1×10^5 s^{-1}. Due to the sharp temperature onset of the observable hole decay and the resulting narrow temperature range, for which decay measurements were possible, the best-fit values for the attempt frequency ν_0 have a resulting rather large experimental error.

C. Spectral holewidth

It was experimentally verified that the spectral holewidth $\Delta\nu_h$ is independent of the spectral hole position within the inhomogeneously broadened absorption line (width $\Gamma_{\rm inh}$). Therefore all hole burning experiments were performed in the absorption maximum for optimum signal-to-noise ratio. The holewidths were obtained in the limit of small burn intensities to avoid power broadening. Also each data point was obtained as an extrapolation to "zero exposure" of a number of nonoverlapping holes burned with decreasing burning times thus avoiding saturation broadening.

The persistent holewidths were seen to depend both on crystal temperature and sample composition. Also, the ratio between $\Delta\nu_h$ and $\Gamma_{\rm inh}$ of the ν_2 transition was seen to depend on the sample composition. To measure the temperature broadening, a spectral hole of moderate depth was burned into the ν_2 transition at the lowest obtainable sample temperature $T=5$ K and its spectral profile was then probed at elevated temperatures $T\geq T_{\rm burn}$. The total transition linewidth $\Gamma_{\rm inh}$ was measured with the FTIR spectrometer in the second harmonic transition when the defect pair concentration was high enough, or otherwise in the (factor 2 narrower) fundamental transition. All these observed dependencies are summarized in Fig. 6 for the K^+:CN^-/CsCl system which has the largest hole stability range of the six

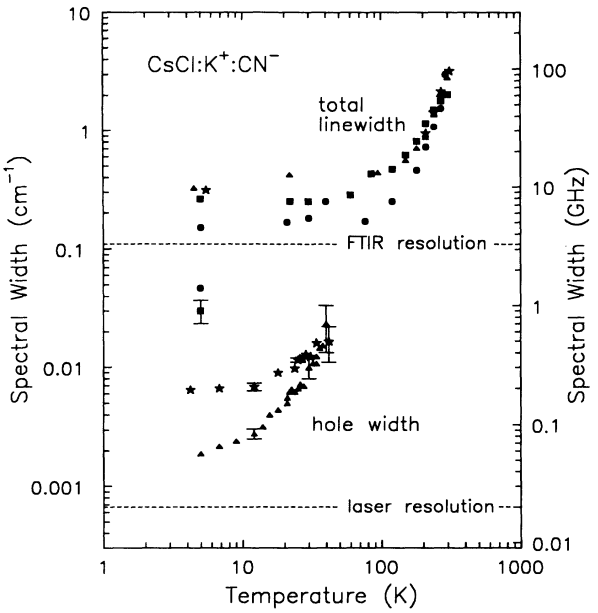

FIG. 6. Temperature broadening of the persistent spectral holewidth and of the inhomogeneously broadened total linewidth for the ν_2 transition of K^+:CN^- defects in CsCl, containing ●: 1×10^{-4} K^+, 3.2×10^{-3} CN^-, and 1.5×10^{-5} K^+:CN^-; ■: 1×10^{-2} K^+, 2.9×10^{-3} CN^-, and 1.0×10^{-3} K^+:CN^-; ★: 2×10^{-2} K^+, 4.4×10^{-4} CN^-, and 3.8×10^{-4} K^+:CN^-; ▲: 2×10^{-2} K^+, 1.8×10^{-4} CN^-, and 1.4×10^{-4} K^+:CN^-.

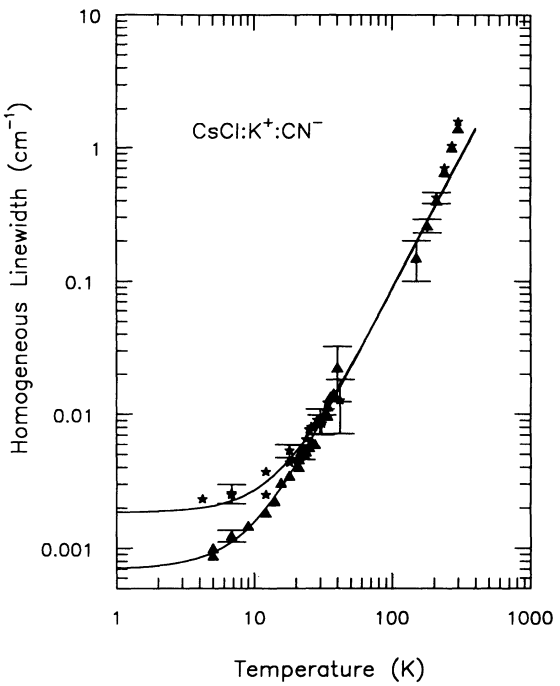

FIG. 7. Temperature dependence of the homogeneous linewidth of the ν_2 transition of K^+:CN^- defects in ★: 2×10^{-2} K^+, 4.4×10^{-4} CN^-, and 3.8×10^{-4} K^+:CN^-; ▲: 2×10^{-2} K^+, 1.8×10^{-4} CN^-, and 1.4×10^{-4} K^+:CN^-. The solid curves are parabolic fits.

defect/host combinations. As seen from the low-temperature (5 K) data, $\Delta\nu_h$ varies by more than an order of magnitude (between 1.8×10^{-3} and 4.7×10^{-2} cm^{-1}) for the indicated sample compositions, while Γ_{inh} varies only by a factor of 3 (from ~0.13 to ~0.3 cm^{-1}). For the sample with the narrowest holes the ratio between holewidth and total linewidth is approximately 1:200. For the sample with the widest holes, the width of the holes approaches that of the total line (ratio $\sim$1:2), thus preventing accurate measurements of holewidth variations with temperature. The specific dependencies on the defect concentrations are discussed in Sec. V. The increase in the observed holewidth with increasing temperatures shown in Fig. 6 is completely reversible in a thermal cycle. This indicates the absence of spectral diffusion processes on the time scale of the cycling experiment. Therefore, the homogeneous linewidth of the transition can be extracted from these data; this is the subject of the following paragraph.

D. The homogeneous linewidth

The homogeneous linewidth $\gamma_{hom}(T)$ of the transition is related to the measured spectral holewidth $\Delta\nu_h(T)$ at any temperature through[17]

$$\Delta\nu_h(T)=\gamma_{hom}(T)+\gamma_{hom}(T_{burn}) , \quad (1)$$

where $\gamma_{hom}(T_{burn})=\frac{1}{2}\Delta\nu_h(T_{burn})$ is the homogeneous linewidth at the burning temperature T_{burn}. Equation (1) is valid under the conditions that $\Delta\nu_h \ll \Gamma_{inh}$ and that the holewidth is not influenced by additional broadening due to long burning times or high light intensities.

Since all these conditions were met, Eq. (1) was used to calculate $\gamma_{hom}(T)$ from the measured holewidths $\Delta\nu_h(T)$ shown in Fig. 6. The laser linewidth (<20 MHz) was not deconvoluted from the measured holewidths. In the high-temperature range ($T>40$ K), where the spectral holes are not persistent anymore, $\gamma_{hom}(T)$ was determined from the total bandwidth $\Gamma_{inh}(T)$ of the ν_2 transition via line-shape deconvolution. For that, it was assumed that the line shape is a Voigt profile and that the inhomogeneous part is independent of temperature. The measurements of these line shapes were performed in the ~50 times stronger fundamental K^+:CN^- ν_2 transition with the FTIR spectrometer.

The result for γ_{hom} versus temperature for two CsCl:K^+:CN^- samples with different CN^- concentrations is shown in Fig. 7. The solid lines are parabolic fits using $\gamma_{hom}=\gamma_0+\beta T^2$. Within experimental error, both curves increase with the same parameter β, while the low-temperature "residual linewidth" γ_0 is notably higher for the sample with the higher CN^- concentration.

V. DISCUSSION

All observed hole burning features (appearance and polarization of antihole, thermal hole and antihole stabili-

ties) appear to be consistent with a burning mechanism where under narrow-linewidth laser excitation the K^+-associated CN^- molecules perform 180° flips between two energetically inequivalent ionic configurations thus creating a spectral hole in the inhomogeneously broadened transition. Due to large barrier heights for reorientation the holes are persistent up to relatively high temperatures (40 K for the K^+:CN^-/CsCl system).

The central results of this investigation are the data shown in Fig. 6, which shows the variation of the width of the persistent spectral holes burned into the ν_2 transition of K^+:CN^- in CsCl both with crystal composition and temperature. Obviously, the observed $\Delta\nu_h$ versus T variation (roughly T^2) is strikingly different from the T^7 temperature variation due to Raman scattering of acoustic phonons in crystalline systems far below the Debye temperature, and it is instead more reminiscent of the dephasing behavior of impurities in glassy systems. Possible candidates for dephasing processes in our systems are pseudolocal modes, internal defect modes, and excitations of the isolated CN^- molecules.

Contributions of isolated K^+ ions to the dephasing are not expected. These unpaired defects, smaller than the replaced Cs^+ ions, distort the lattice in their vicinity and should only introduce a *static* stress distribution into the crystal. This should only affect the inhomogeneous broadening of the K^+:CN^- transitions. Furthermore, any potential dynamic motion of the isolated light K^+ defects should give rise to a local mode above the optical branch of the phonon spectrum (larger than 200 cm^{-1}). Since this mode would be thermally populated only outside of the stability range of the spectral holes, no participation of the K^+ defects in the lattice dynamics and hence in the dephasing is to be expected.

A much more likely contributor to dephasing are isolated CN^- molecules. Their rapid reorientational motion on their lattice sites should introduce fluctuating strain fields into the sample which in turn might modulate the eigenfrequency of the rotationally aligned K^+:CN^- pair defects via elastic interaction. The magnitude of these modulations and their influence on the dephasing can be expected to increase with increasing concentration of the isolated CN^- molecules.

A further potential contributor to dephasing are lattice phonons with a non-Debye-like phonon density of states. A comparison of the $\gamma_{\rm hom}$ versus T functional dependence with phonon dephasing theories[18–22] should help to identify the nature of these phonons (e.g., participation of pseudolocal modes).

Lifetime (T_1) contributions to the homogeneous linebroadening can be ruled out. The relation between $\gamma_{\rm hom}$ and the excited state lifetime T_1 is[23]

$$\gamma_{\rm hom}=\frac{1}{2\pi T_1}+\frac{1}{\pi T_2^*}\ , \tag{2}$$

where T_2^* is the pure dephasing time. For the K^+:CN^- pair defects T_1 was measured in the μs-ms range,[24] corresponding to a lifetime contribution to $\gamma_{\rm hom}$ on a sub-MHz level. Compared to the measured values this is at least one order of magnitude smaller. Therefore the measured data reflect the pure dephasing behavior of the excited state.

A further parameter to the line broadening is the defect concentration(s) in the sample. As is apparent from Fig. 6 and also from Fig. 7, the residual low-temperature linewidths differ by a factor of 2–10 for the shown cases. On the other hand, the linewidth data at higher temperatures appear to be sample independent.

A. The residual linewidth

Since the isolated CN^- molecules perform rapid reorientations on their lattice sites even at the lowest temperatures, a line-broadening mechanism involving the abundant isolated CN^- molecules is conceivable. We will argue that it is indeed the isolated CN^- molecules which are involved in the mechanism and cause the residual broadening via dynamic elastic dipole-dipole interaction with the K^+:CN^- defects.

The correlation between the homogeneous broadening at the lowest temperatures and the concentration of isolated CN^- molecules is evident from Fig. 8. Here $\gamma_{\rm hom}$ is plotted both versus the concentration $n_{K^+:CN^-}$ of the K^+:CN^- pair defects [Fig. 8(a)] and versus the concentration n_{CN^-} of the isolated CN^- molecules [Fig. 8(b)]. In one sample class (labeled "2% K^+") the CN^- doping was varied from 1×10^{-4} to 5×10^{-3} while the K^+ doping was kept near the solubility limit of 2%. This maximized the ratio of $n_{K^+:CN^-}/n_{CN^-}$. In another class (labeled "$[K^+]/[CN^-]=2:1$") both the K^+ and the CN^- doping was varied in a fixed 2:1 ratio; in this case $n_{K^+:CN^-}/n_{CN^-}$ is reduced by roughly one order of magnitude. A further data point was obtained for a sample in which the K^+ doping was about a factor 50 smaller than the CN^- doping. When $\gamma_{\rm hom}$ is plotted versus $n_{K^+:CN^-}$ [Fig. 8(a)], totally different linewidths are obtained in samples with the same $n_{K^+:CN^-}$ but different n_{CN^-}. However, when $\gamma_{\rm hom}$ is plotted versus n_{CN^-} [Fig. 8(b)], a smooth dependence is obtained, even though $n_{K^+:CN^-}$ can vary between samples with the same n_{CN^-} by as much as one order of magnitude.

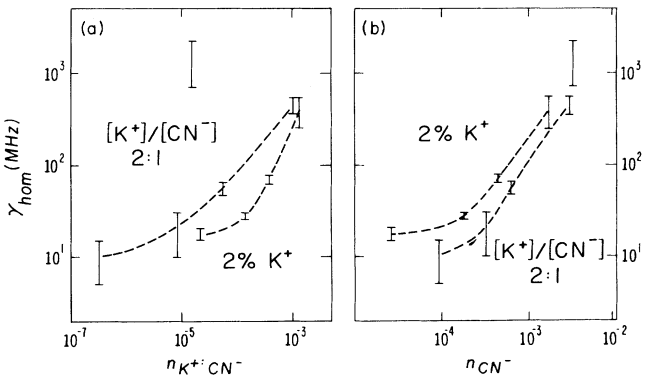

FIG. 8. Homogeneous linewidth of ν_2 transition of K^+:CN^- defects in various CsCl samples at $T=5$ K vs (a) the K^+:CN^- defect concentration and (b) the isolated CN^- concentration.

1. The elastic dipole model

In order to obtain the dependence of γ_{hom} on n_{CN^-} quantitatively, we describe the interaction between the isolated CN^- molecules and the K^+:CN^- defect pairs in terms of an "elastic dipole" model. We treat the isolated CN^- molecules as a dynamic source of lattice deformations, i.e., dynamic strain fields. Both the isolated CN^- molecules and the K^+:CN^- pair defects are modeled as elastic dipoles which interact through elastic strain fields. Ignoring any *static* strain components from other impurities and assuming adiabatic conditions, the transition frequency of a K^+:CN^- defect at a given time would then depend on the orientation of the isolated CN^- molecules in its vicinity. Any reorientation of the isolated CN^- molecules would then modulate the transition frequency of the K^+:CN^- defects. Since the reorientational motion of the isolated CN^- molecules happens on a sub-ns time scale (expected from a tunnel splitting of $\sim$1–2 cm^{-1}),[11] the relatively slow hole burning technique measures the envelope of all frequency excursions, i.e., an average "dynamic strain broadening." Different K^+:CN^- defects experience different strain fields depending on their different local environments (different distances to the neighboring isolated CN^- molecules). The measured homogeneous linewidths therefore reflect an ensemble average rather than a site-independent constant quantity.

We derive now an expression for the strain field of an elastic dipole, then determine the strain field fluctuations for an ensemble of elastic dipoles, and finally calculate the transition energy broadening for a K^+:CN^- defect pair subjected to these fluctuations.

Within the concept of an elastic dipole,[25,26] the elastic deformation of the lattice around a defect is expressed by the elastic dipole tensor λ, and the elastic energy u_p of the elastic dipole in a stress field σ is given by

$$u_p = -v_0 \lambda_{ij}^{(p)} \sigma_{ij} \ . \tag{3}$$

Here (p) denotes the specific crystallographic orientation of the elastic dipole, and v_0 is a normalizing volume, usually taken as the unit cell volume of the lattice, so that the $\lambda_{ij}^{(p)}$ are dimensionless.

With Eq. (3) the elastic energy u_p of a K^+:CN^- defect (at $\mathbf{r}_0$) in the vibrational state $|n\rangle$ is given by

$$u_p = -v_0 \lambda_{ij}^{(p,n)} \sigma_{ij}(\mathbf{r}_0) \ , \tag{4}$$

so that the transition energy $h\nu$ of the second harmonic can be written as

$$\begin{aligned} h\nu &= = E_{\text{vib}} - v_0(\lambda_{ij}^{(p,2)} - \lambda_{ij}^{(p,0)})\sigma_{ij}(\mathbf{r}_0) \\ &= E_{\text{vib}} - v_0 D_{ij}^{(p)} \sigma_{ij}(\mathbf{r}_0) \ . \end{aligned} \tag{5}$$

Here E_{vib} is the transition energy in an undeformed lattice under absence of any applied stress, and $D^{(p)}$, the coupling tensor, is defined as the change of the K^+:CN^- elastic dipole tensor upon vibrational excitation; the latter will be treated as a parameter which in principle can be determined by a uniaxial experiment. The stress σ is related to the strain ϵ by

$$\sigma_{ij}(\mathbf{r}) = c_{ijlm} \epsilon_{lm}(\mathbf{r}) \ , \tag{6}$$

where c is the elastic modulus tensor (see Appendix A), so that we finally have

$$h\nu = E_{\text{vib}} - v_0 D_{ij}^{(p)} c_{ijlm} \epsilon_{lm}(\mathbf{r}_0) \ . \tag{7}$$

We continue now with an evaluation of the strain ϵ and the coupling tensor D within the elastic dipole model. For substitutional elastic point defects, like isolated CN^- molecules, the strain fields are inhomogeneous. In order to obtain the spatial dependence of the strain fields for this case we follow a model calculation by Black and Halperin[27] and equate the (external) stress force at the CN^- elastic dipole site $\mathbf{r}=\mathbf{0}$ to the internal stress forces in the crystal:[28]

$$v_0 c_{ijlm} \lambda_{lm} \partial_j \delta(\mathbf{r}) = \rho c_t^2 \nabla^2 u_i + \rho(c_l^2 - c_t^2)\partial_i(\partial_\nu u_\nu) \ . \tag{8}$$

Here c_t and c_1 are the transversal and longitudinal sound velocities of the crystal, ρ its mass density, and $\mathbf{u}$ the displacement vector of the lattice sites due to the stress σ. The values for these quantities are given in Appendix A.

With the strain field $\epsilon(\mathbf{r})$ related to the lattice displacement $\mathbf{u}(\mathbf{r})$ by

$$\epsilon_{lm}(\mathbf{r}) = \tfrac{1}{2}[\partial_l u_m(\mathbf{r}) + \partial_m u_l(\mathbf{r})] \ , \tag{9}$$

the result for the strain field generated by the CN^- elastic dipole is given by

$$\begin{aligned} \epsilon_{lm}(\mathbf{r}) = v_0 \frac{1}{|\mathbf{r}|^3} \frac{1}{8\pi\rho} \Bigg\{ & \frac{2}{c_l^2} c_{lmik} \lambda_{ik} + 3\left[\frac{1}{c_t^2} - \frac{2}{c_l^2}\right]\left[\frac{r_l r_k c_{mk\alpha\beta}\lambda_{\alpha\beta} + r_m r_k c_{lk\alpha\beta}\lambda_{\alpha\beta}}{|\mathbf{r}|^2}\right] \\ & + \left[\frac{1}{c_t^2} - \frac{1}{c_l^2}\right]\left[\left[-\delta_{lm} + \frac{3 r_l r_m}{|\mathbf{r}|^2}\right] c_{\nu\nu\alpha\beta}\lambda_{\alpha\beta} + 3\left[\delta_{lm} - \frac{5 r_l r_m}{|\mathbf{r}|^2}\right]\frac{r_\alpha r_\beta c_{\alpha\beta\gamma\delta}\lambda_{\gamma\delta}}{|\mathbf{r}|^2}\right]\Bigg\} \ . \end{aligned} \tag{10}$$

Here the origin of the coordinate system is placed at the site of the elastic dipole. The derivation holds strictly only for an isotropic elastic continuum; no closed expressions can be given for the elastic dipole field in a cubic crystal.[29]

As seen from Eq. (10) the strain field around the elastic dipole has r^{-3} dependence. Since the average distance $\langle r \rangle$ from an arbitrary site in the crystal to the nearest

impurity with concentration n is proportional to $n^{-1/3}$, the amplitude of the strain modulation and therefore the homogeneous linewidth is expected to be directly proportional to the concentration n_{CN^-} of the isolated CN^- molecules. This behavior is indeed observed in Fig. 8(b), where a double-logarithmic plot of γ_{hom} versus n_{CN^-} reveals a slope of ~ 1.

In order to calculate the strain field $\epsilon(\mathbf{r})$ around an isolated CN^- molecule with Eq. (10), the elastic dipole tensor λ is needed. While this has not been measured for isolated CN^- defects in cesium halide hosts, we estimate this tensor as (Appendix B)

$$\lambda \approx 0.15 \begin{bmatrix} 1 & 0 & 0 \\ 0 & 0 & 0 \\ 0 & 0 & 0 \end{bmatrix} . \tag{11}$$

2. *Model calculations for the strain broadening*

With Eqs. (7) and (10) the transition frequency $\nu(\epsilon)$ can be calculated for a single K^+:CN^- pair defect in the strain field $\epsilon(\mathbf{r})$ of a single isolated CN^- molecule having arbitrary orientation. In order to calculate the homogeneous linewidth γ_{hom}, the average strain field fluctuation caused by the reorientational motion of an *ensemble* of isolated CN^- molecules is needed. Therefore we would have to calculate the dynamic strain broadening $\Delta\nu$ via

$$\begin{aligned}(\Delta\nu)^2 &= \langle (\nu - \langle \nu \rangle)^2 \rangle \\ &= \langle \nu^2 \rangle - \langle \nu \rangle^2 ,\end{aligned} \tag{12}$$

where $\langle \cdots \rangle$ denotes a suitable averaging over all spatial distributions of isolated CN^- dipoles. According to Eq. (12) this would involve the averaging of quadratic terms of the superposition of a large number of strain fields calculated with Eq. (10). Rather than performing this tedious calculation we used Eqs. (7) and (10) for a Monte Carlo simulation.

For that we considered a single [111] oriented K^+:CN^- defect positioned in the center of a three-dimensional lattice. A certain number of $\langle 111 \rangle$ elastic CN^- dipoles was then randomly distributed on an appropriate number of lattice sites around it (matching the experimentally used concentrations). The stress field $\sigma(\mathbf{0})$ at the site of the K^+:CN^- defect was finally obtained as a linear superposition of the stress fields $\sigma_i(\mathbf{r})$ of the CN^- elastic dipoles at $\mathbf{r}_i$, which were calculated with Eqs. (10) and (6). To simulate the fluctuating stress field of the reorienting CN^- elastic dipoles, $\sigma(\mathbf{0})$ was calculated for several independently generated different $\langle 111 \rangle$ orientations of the dipoles, and this process was then iterated for a large number of random spatial distributions of the dipoles.

Figure 9 shows the axial stress distribution for a K^+:CN^- pair defect calculated in this way for a concentration of isolated CN^- molecules of 1.8×10^{-4} (matching one of our samples). For this result 1000 random spatial distributions were generated (24 elastic dipoles on a $51\times51\times51$ grid) and for each spatial distribution the stress was calculated for 15 random elastic dipole orientations.

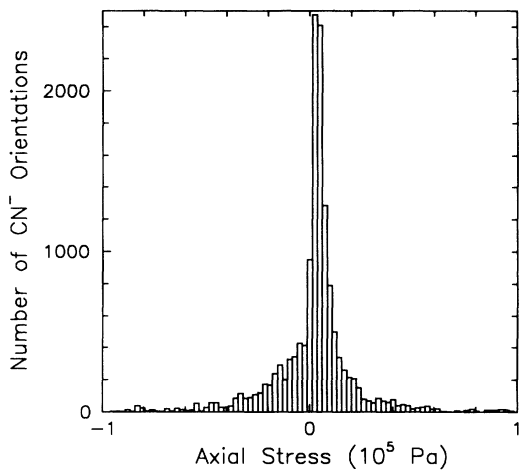

FIG. 9. Dynamic axial stress distribution at a K^+:CN^- pair defect site in a CsCl lattice caused by the fluctuating strain fields of tunneling isolated CN^- elastic dipoles. Shown is the number of equivalent CN^- configurations calculated for the indicated axial stress values by Monte Carlo simulation (see text).

Due to the axial symmetry of the K^+:CN^- defect we assume that only the axial stress component has to be considered for the broadening of the K^+:CN^- transition frequency, i.e., $h\nu \propto D_{11}\sigma_{11}$. With the width of the calculated distribution in Fig. 9 the transition broadening can then be calculated with Eq. (5).

From Fig. 9 the width of the simulated dynamic stress distribution for a CsCl sample with 2×10^{-2} K^+ mol parts, 1.8×10^{-4} isolated CN^-, and 1.4×10^{-4} K^+:CN^- is 0.1 bar. An order-of-magnitude estimation for D_{11} (see Appendix C) gives a value of $\sim 3\times10^{-3}$. With Eq. (5) the dynamic strain broadening γ_{hom} is calculated as 3 MHz.

As discussed in Sec. V C, an additional contribution to the homogeneous linewidth is due to dephasing by low-frequency non-Debye lattice modes. Their contribution to linewidth broadening at $T=5$ K is about 3 MHz. This taken into account, we have agreement between the experimentally observed 28 ± 3 MHz linewidth value and the 6-MHz value predicted by our models within a factor of 4–5.

Uncertainties in the elastic dipole model calculation are the estimates for the D and λ values, but also the validity of this elastic continuum model itself, which might underestimate the elastic dipole-dipole coupling. In fact, it has been shown that the strain field around an elastic dipole has a larger $r^{-5/2}$ range compared to r^{-3} if instead of an elastic continuum model a phonon model with a modified Debye spectrum is used.[30]

B. The inhomogeneously broadened linewidth

Besides using the elastic dipole model for an estimate of the low-temperature homogeneous linewidth we use

the same model also to discuss its consequences for the total inhomogeneously broadened transition width Γ_{inh}. For this inhomogeneous strain broadening the lattice deformations produced by the abundant isolated *static* K^+ impurities as well as the *static* contributions of the isolated CN^- molecules have to be considered, whereas the influence of the K^+:CN^- pair defects can be neglected due to their low concentration levels.

The small K^+ ion (compared to Cs^+) causes a static contraction of the lattice around the K^+ site. With an ionic radius of 1.33 Å for K^+ and 1.81 Å for Cl^-, a rigid-sphere assumption yields a defect cell dimension of 3.63 Å, compared to the 4.12-Å unit cell for the unperturbed CsCl host crystal. With this, the elastic dipole tensor λ_{K^+} can be obtained. For a spherically symmetric defect, the tensor is given by $\lambda_{ij}=\lambda\cdot\delta_{ij}$. Since the size factor $\Delta v_0/v_0$ is given by[28] $\Delta v_0/v_0=\mathrm{tr}(\lambda)=-0.32$, we have $\lambda_{K^+}=-0.11$.

The *isotropic* component λ_{CN^-} of the CN^- elastic dipole equals +0.05 (see Appendix B). That means that the distortion of the lattice around a K^+ defect is about twice as strong and of opposite sign compared to the *static* distortion around an isolated CN^- molecule.

The inhomogeneous component of the transition linewidth should then be related to a suitable average of both dopant concentrations. If we assign to the K^+ concentration a statistical weight of one, the CN^- concentration has to be weighted according to the ratio of the size factors ($=|\lambda_{CN^-}/\lambda_{K^+}|$). Figure 10 shows a plot of the inhomogeneous component Γ ($=\Gamma_{inh}-\gamma_{hom}$) of the K^+:CN^- ν_2 transition at $T=5$ K as a function of the weighted impurity concentrations. The clear correlation between concentration and broadening indicates that impurity doping is indeed a major contributor to the inhomogeneous K^+:CN^- linewidths in the CsCl samples. Fitting the curve to a power law, the exponent varies between 0.4 and 0.65 over the measured concentration range. If the strain fields of the considered impurities were the only source of the inhomogeneous broadening, a slope of one would be expected.

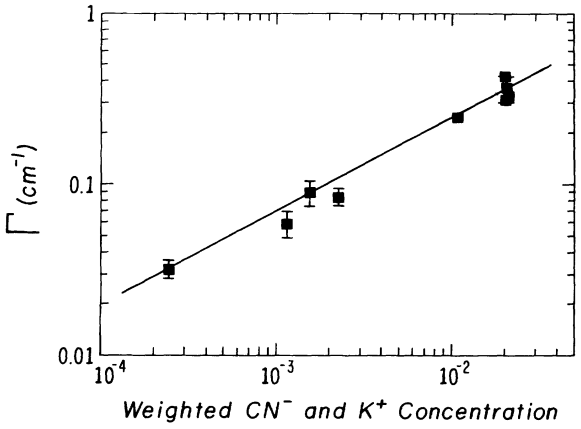

FIG. 10. Width of the inhomogeneous component of the ν_2 transition of K^+:CN^- defects in CsCl vs weighted concentrations (see text) of isolated CN^- and K^+ impurities.

An elastic dipole model calculation was then carried out for the static stress field of the isolated K^+ impurities. For a K^+ concentration of 2×10^{-2} (same sample as used in the Monte Carlo simulation above), 69 elastic spheres were distributed on a $15\times15\times15$ grid. The concentration of the isolated CN^- molecules (1.8×10^{-4}) was negligible for this simulation. The results for the axial stress component considering 5000 K^+ distributions is shown in Fig. 11. The width of the calculated stress distribution is approximately 15 bar, which according to Eq. (5) would correspond to an inhomogeneous broadening of 0.5 GHz. For a sample with that K^+ concentration the *experimental* value Γ for the inhomogeneous broadening is 9.75 ± 0.25 GHz.

A close look at Fig. 11 shows that the envelope of the stress distribution is slightly offset from zero by ~-4 bar. This stress corresponds to a K^+:CN^- transition energy increase of $\sim4\times10^{-3}$ cm^{-1} (130 MHz). For CsCl samples with 2% K^+ concentration a transition energy increase of ~0.05 cm^{-1} was experimentally observed compared to samples with low (10^{-4} mol parts) K^+ concentration. Similarly, a high isolated CN^- concentration in a sample leads to a positive stress offset (as seen from Fig. 9) and a corresponding transition energy shift to lower energies. This effect was experimentally observed when comparing samples with about the same K^+ level but largely varying isolated CN^- concentrations.

The elastic dipole model explains qualitatively the dependence of the inhomogeneous broadening and the transition energy shift on the impurity concentrations. Similarly to the dynamic case, the elastic continuum model again underestimates the magnitude of the effects, i.e., the coupling of the K^+:CN^- elastic dipoles to the static strain fields in the samples. However, as sources for the latter only K^+ and CN^- defects were considered and potentially existing other sources (dislocations, microvoids, other accidental impurities) were neglected.

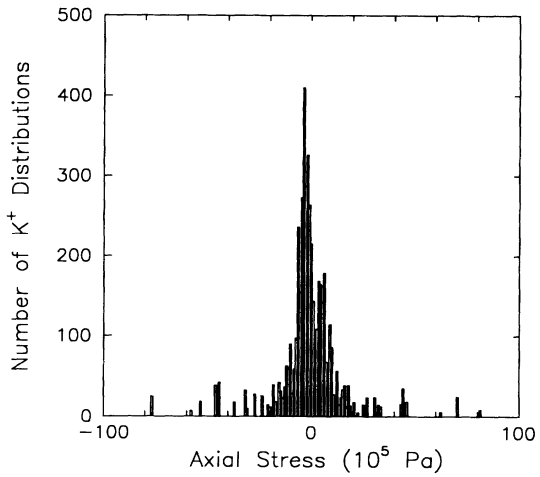

FIG. 11. Static axial stress distribution at a K^+:CN^- pair defect site in a CsCl lattice caused by isolated K^+ impurities. Shown is the number of equivalent K^+ configurations calculated for the indicated axial stress values by Monte Carlo simulation (see text).

C. Temperature broadening of γ_{hom}

The dynamic behavior of the isolated CN^- molecules changes with increasing temperatures from tunneling between the ⟨111⟩ equilibrium orientations to hindered rotation and quasifree rotation.[10,11,31] For isolated CN^- molecules in CsCl quasifree rotation has been observed for temperatures above ~120 K, so that the rotational barrier height could be estimated[32] to be ~85 cm^{-1}. The question arises, whether the temperature broadening of the homogeneous linewidth of the K^+:CN^- transition is connected with the changing CN^- dynamics. Associated with temperature increase is an increase in the strain fluctuation frequency. Within the assumptions of our adiabatic elastic dipole model, however, only the fluctuation *amplitude* but not the fluctuation frequency has an influence on the width of the K^+:CN^- transitions. In this section we will discuss the contribution of phonons which at $T \neq 0$ have to be considered as sources of dynamic lattice strain.

Homogeneous line broadening due to coupling of defects to lattice phonons has been comprehensively treated and reviewed by Skinner and co-workers.[18–22] We will compare the predictions of their theory for several simple phonon density-of-states models with the observed experimental behavior. From this comparison we will try to decide whether any lattice phonons can account for the observed broadening, and if so, which type of phonons (acoustic, optic, pseudolocal modes).

The vibration eigenfrequency of the K^+ associated CN^- molecules (~2000 cm^{-1}) is far above the maximum phonon frequency of the lattice (~200 cm^{-1}), so that the assumption of weak vibration/phonon coupling ($W \ll 1$) appears justified. This is experimentally supported by the absence of any strong phonon sidebands to the K^+:CN^- ν_1 and ν_2 transitions. Therefore we compare our experimental data with the theoretical results for the weak coupling limit.

1. *Acoustic phonons*

If we are primarily concerned with the homogeneous line broadening in the low temperature range ($T \leq 40$ K), we can assume that the acoustic phonons are solely responsible for the line broadening and we can neglect the higher-frequency optical branch ($\omega_{op} \geq 2 \times 10^{13}$ rad/s). If the acoustic phonons are treated in the Debye approximation, the line broadening (FWHM in Hz) is given by[19]

$$\gamma_{hom} = \omega_D \frac{9W^2}{4} \left[\frac{T}{T_D} \right]^7 \int_0^{T_D/T} dx \frac{x^6 e^x}{(e^x - 1)^2} , \qquad (13)$$

where T_D is the Debye-temperature and ω_D is the phonon cutoff frequency ($\hbar\omega_D = kT_D$). Within this model the holewidth displays a T^7 behavior at $T \ll T_D$ and a T^2 behavior for $T \gg T_D$. A comparison of the experimental data for $\gamma_{hom}(T)$ with γ_{hom} according to Eq. (13) is given in Fig. 12. With a Debye-temperature of 165 K for a CsCl crystal,[33] the coupling constant W and the low-temperature residual linewidth were obtained from a nonlinear best fit to the data. The functional dependence γ_{hom} versus T is shown as a dashed line in Fig. 12. The deviation of the data from the expected behavior is quite obvious. This indicates that the Debye model is a poor approximation for the actual phonon density in the crystal. The fit improves considerably if the Debye temperature is treated as an additional free parameter. With a resulting $T_D \approx 40$ K, the curve shown as a solid line in Fig. 12 results as a fit to the data. However, nothing justifies this specific Debye temperature as can be seen from a comparison of the phonon density according to a Debye model with $T_D = 40$ K and the actual phonon density of a *pure* CsCl crystal, shown in Fig. 13: there is no significant overlap of the phonon densities in any frequency range.

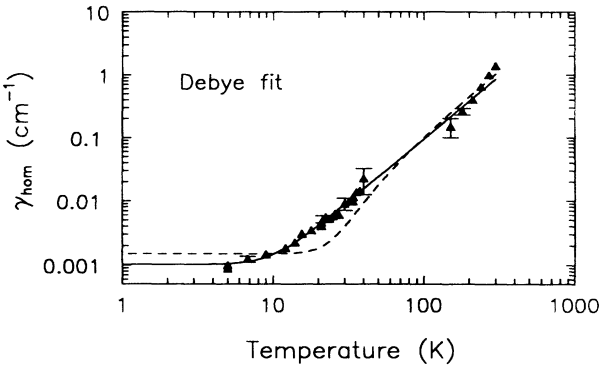

FIG. 12. Variation of γ_{hom} of the ν_2 transition of K^+:CN^- defects in CsCl with T. The concentration of isolated CN^- molecules is 1.8×10^{-4}. The dashed curve is a Debye fit to the data with $T_D = 165$ K (Ref. 33). The solid curve is a fit with $T_D = 40$ K, obtained when treating T_D as a free parameter in the fit.

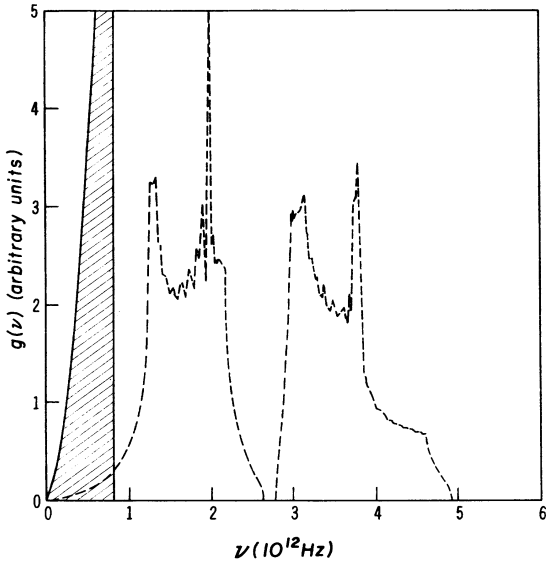

FIG. 13. Phonon density of states for a CsCl lattice as measured by neutron diffraction [after Ahmad *et al.* (Ref. 33)]. Superimposed and shown as solid line is the phonon density of states according to a Debye temperature T_D of 40 K.

2. *Pseudolocal mode*

If the substitution of an impurity leads to a sizable perturbation of the lattice (mass mismatch, or strong change of force constants), additional normal modes are introduced to the crystal.[34] An impurity mode above the optical band (local mode) or in the gap region (gap mode) is sharply peaked and does not contribute to dephasing.[19] If the frequency of the impurity mode falls into the acoustic or into the optical band, it can become delocalized by mixing with band phonons and a resonant or "pseudolocal" mode is created. The resulting phonon density of states can substantially differ from the unperturbed spectrum, so that neither the Debye nor the Einstein model are adequate approximations. We will analyze our data with the simplest phenomenological model for a low-frequency pseudolocal mode at ω_0 in the acoustic band. For a quasi-Lorentzian phonon density of states the result for the homogeneous linewidth (FWHM in Hz) in the weak coupling limit is[20,22]

$$\gamma_{\rm hom}=\frac{W^2}{4\pi}\omega_0^2\tau_0 n(\omega_0)[n(\omega_0)+1]\ , \tag{14}$$

where $1/\tau_0$ is the FWHM of the phonon density distribution ($\omega_0\cdot\tau_0\gg 1$), ω_0 is the pseudolocal mode frequency, and $n(\omega_0)$ the average thermal phonon occupation number. A best fit according to Eq. (14) for two CsCl samples is shown in Fig. 14. The free parameters are the pseudolocal mode frequency ω_0, the coupling factor $W^2\tau_0$, and the residual linewidth $\gamma_{\rm hom}(0)$. Only the low-temperature data points ($T\leq 40$ K) were fitted. While the fit gives 9 and 10 $\rm cm^{-1}$ for ω_0, good agreement with the data is also obtained for ω_0 in the range 5–20 $\rm cm^{-1}$. This large uncertainty results from the obstruction of the linewidth variation at the lowest temperatures by the large residual component.

At higher temperatures ($T\geq 40$ K), the optical phonons become thermally populated as well, so that systematic deviations of the fit in this range are to be expected. This seems to be confirmed by the larger slope of the experimental data points in Fig. 14 in this temperature range. The low-temperature data, on the other hand, are consistent with the presence of a ~ 10 $\rm cm^{-1}$ excitation in the crystal. The absolute value of the homogeneous broadening at the lowest measured temperature of 5 K due to dephasing by the pseudolocal mode is about 3 MHz according to the fit. This value is in the same range as the contribution to broadening by the dynamic dipole-dipole interaction (see Sec. V A).

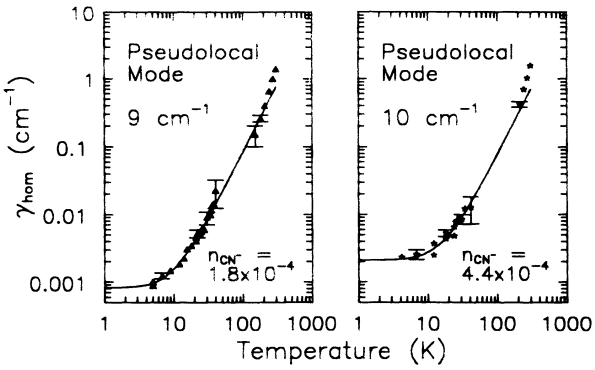

FIG. 14. Variation of $\gamma_{\rm hom}$ of the ν_2 transition of K^+:CN^- defects in CsCl with T for two different concentrations of isolated CN^- molecules, 1.8×10^{-4} (▲), 4.4×10^{-4} (★). The solid curves are fits to the data with a pseudolocal mode model (see text) resulting in a pseudolocal mode frequency of ~ 10 $\rm cm^{-1}$ in both cases.

The nature of this mode is unclear at present. Both the isolated CN^- molecules and the K^+:CN^- pair defects themselves are potential sources. The elastic dipole model for the residual line broadening related the dephasing of the K^+:CN^- defects to differences in stress produced by the eight possible ⟨111⟩ orientations of the isolated CN^- molecule. For the CN^- molecular reorientations a pure tunneling process was assumed and any coupling to lattice phonons was neglected. These assumptions appear justified at $T\rightarrow 0$. Toward higher temperatures, where phonon-assisted tunneling, libration and hindered rotation of the CN^- molecules occur, this simple picture does not necessarily apply anymore. The CN^- molecule then has a finite probability for orientations other than the ⟨111⟩ crystal directions, so that the dynamic strain fluctuations could have a higher amplitude. Also, a librational impurity mode within the acoustic band of a crystal can of course couple with acoustic phonons and thus create a corresponding peak in the phonon density of states. This cannot be ruled out for substitutional CN^- molecules in CsCl, which are known to have a weak librational sideband (~ 20 $\rm cm^{-1}$ shift) to their vibrational transitions.[35]

Another possible origin for a pseudolocal mode are the K^+:CN^- pair defects themselves. If the K^+:CN^- complex is pictured as a linear triatomic molecule, it has 3N-3-2=4 normal modes, two of which correspond to a librational motion of the CN^- unit, one to the (slightly perturbed) CN^- stretch vibration at ~ 2000 $\rm cm^{-1}$, and one to a translational motion of the CN^- toward the stabilizing K^+ ion. Since the rotational alignment of a K^+:CN^- pair points to a much steeper librational potential than for an isolated CN^- molecule, the librational frequency of the K^+:CN^- pair can be expected to be somewhat higher than the ~ 20 $\rm cm^{-1}$ value observed for isolated CN^- defects. It is conceivable, however, that the K-CN stretch mode has a low frequency. The CN^- eigenfrequency is only slightly perturbed ($\lesssim 0.5\%$), when the CN^- is associated with the stabilizing K^+ ion, so that a much weaker K-CN bond compared to the C-N bond and hence a low frequency for the K-CN stretch vibration can be expected. If a K^+:CN^- internal translational mode is indeed responsible for the temperature broadening of the K^+:CN^- homogeneous linewidth, the perturbation of the CN^- eigenfrequency happens locally, so that the broadening of $\gamma_{\rm hom}$ should be independent of the K^+:CN^- and of the CN^- concentration in the samples. This seems to be supported by the experimental evidence shown in Fig. 7 where the homogeneous linewidth $\gamma_{\rm hom}$ in two different samples converges to the same values at higher temperatures. These experiments had to be limited, however, to a small concentration range (be-

tween 1.8×10^{-4} and 4.4×10^{-4} for the concentration of the isolated CN^- molecules). At higher CN^- concentrations, where the spectral holewidth approaches the total transition linewidth, an accurate determination of the spectral holewidth becomes difficult, even more so at elevated temperatures. Low CN^- doping, on the other hand, implies low K^+:CN^- concentrations and prohibitively low signal/noise ratios.

VI. CONCLUSION

K^+:CN^- (and Rb^+:CN^-) pair defects in cesium halides provide a whole class of materials suitable for ir persistent vibrational hole burning studies. The homogeneous linewidth, investigated in detail for K^+:CN^- pair defects in CsCl, displays a broadening at the lowest temperatures which is much stronger than would be expected from lifetime broadening alone. With increasing temperatures it displays a T^2 dependence.

In our proposed elastic dipole model the residual line broadening at low temperatures (5 K) can be explained by "dynamic strain broadening," which is caused by the motional behavior of isolated CN^- molecules. At this temperature these molecules tunnel rapidly between their eight equivalent $\langle 111 \rangle$ orientations separated by low barriers. The fluctuating strain field produced by this dynamics couples the CN^- elastic dipoles to the fixed K^+:CN^- elastic dipoles and therefore causes a strong temperature independent contribution to the broadening of the K^+:CN^- vibrational transitions.

The variation of the homogeneous linewidth with T^2 in the temperature range 5–40 K is attributed to Raman scattering of phonons with a non-Debye effective phonon density of states peaking at ~10 cm^{-1}. This low-frequency excitation could possibly be connected again to the motional behavior of the isolated CN^- molecules which are known to perform librations and hindered rotations in this temperature range. This possibility is supported by the known existence of a librational band in the vibrational spectra of isolated CN^- molecules in CsCl which has approximately the right shift, i.e., ~20 cm^{-1}. Another possibility which cannot be ruled out is coupling of the K^+:CN^- transition to a low-frequency internal translational mode of the K^+:CN^- defect itself (pseudolocal mode).

ACKNOWLEDGMENTS

We would like to acknowledge helpful discussions with B.G. Dick concerning the elastic continuum model. This research was supported by NSF Grant No. DMR 87-06416 and ONR Grants N 00014-91-C-0104 and N 0014-90-C-0035.

APPENDIX A: ELASTIC CONSTANTS FOR CsCl

For a cubic lattice the elastic dipole tensor reduces to three independent elastic constants c_{11}, c_{12}, and c_{44}. Their values and other needed material constants for CsCl are given in Table I.

TABLE I. Bulk parameters for CsCl (from Ref. 36).

Elastic tensor components	c_{11}:	3.66×10^{10} N/m^2
	c_{12}:	9×10^{9} N/m^2
	c_{44}:	8×10^{9} N/m^2
Longitudinal sound velocity	c_l:	2.8×10^{3} m/s
Transversal sound velocity	c_t:	1.6×10^{3} m/s
Lattice parameter	a_0:	4.12×10^{-10} m
Unit-cell volume	v_0:	6.99×10^{-29} m^3
Mass density	ρ:	3.99×10^{3} kg/m^3

APPENDIX B: THE CN^- ELASTIC DIPOLE TENSOR

Expressed in the principal axis system of the elastic defect, the elastic dipole tensor takes on the diagonal form $\lambda_{ij}=\lambda_i\cdot\delta_{ij}$. For the axial-symmetric molecule CN^- in an alkali halide host, $\lambda_2=\lambda_3$. Measurable quantities are the shape factor $\lambda_1-\lambda_2$ and the size factor $\lambda_1+2\lambda_2$ of the elastic defect. These values have not yet been experimentally determined for substitutional CN^- defects in cesium halide hosts.

Concerning the shape factor we relate its value to the value of the same defect in a KCl lattice. For the latter a shape factor 0.15–0.20 has been measured.[37,38] Correcting for the different unit cell volume v_0 [see Eq. (3)] in CsCl, we then estimate the shape factor for CN^- defects in CsCl to $\lambda_1-\lambda_2=0.15$.

The size factor $\lambda_1+2\lambda_2$ for CN^- in CsCl can be assumed to closely resemble the size factor for Br^- in a Br^- sublattice. The reason for this is that the (lattice size dependent) CN^- vibrational eigenfrequency in a cesium bromide host is nearly identical to the corresponding cesium cyanide molecular crystal. Since the unit cell volume v_0 in CsBr is about 14% larger than in CsCl, we estimate the Br^- and thus the CN^- size factor in CsCl to $\lambda_1+2\lambda_2=0.14$.

With these values the CN^- elastic dipole tensor in CsCl is approximated by

$$\lambda\approx0.15\begin{bmatrix}1&0&0\\0&0&0\\0&0&0\end{bmatrix}=\begin{bmatrix}0.05&0&0\\0&0.05&0\\0&0&0.05\end{bmatrix}+\begin{bmatrix}0.10&0&0\\0&-0.05&0\\0&0&-0.05\end{bmatrix}, \tag{B1}$$

where the tensor has been separated into an isotropic and an anisotropic part. When expressed in the crystal coordinates, the isotropic component describes a minor (5%) static outward deformation of the lattice unit cell at the defect while the anisotropic component contains the orientation-dependent deformation of the lattice.

APPENDIX C: THE COUPLING TENSOR D

Information about the coupling tensor D can in principle be gained from a hydrostatic or uniaxial pressure experiment. For a hydrostatic pressure p the stress σ is given by $\sigma_{ij}=-p\delta_{ij}$. Inserting this into Eq. (5), the frequency shift $\Delta\nu$ is related to the applied pressure p through

$$\begin{aligned} h\,\Delta\nu &= -\nu_0 D_{ij}\sigma_{ij} \\ &= \nu_0 D_{ij}\delta_{ij}p \\ &= \nu_0 \mathrm{tr}(D)p \\ &= \nu_0(\Delta\lambda_1+2\,\Delta\lambda_2)p\ , \end{aligned} \tag{C1}$$

where the index for the defect orientation has been suppressed. If we make the reasonable assumption that the axial stress component dominates the induced frequency shift, we have

$$h\,\Delta\nu \approx \nu_0\,\Delta\lambda_1 p\ . \tag{C2}$$

This relation can then be used to determine the dominant coupling tensor eigenvalue $\Delta\lambda_1$ from the measured pressure-induced frequency shift $\Delta\nu$. Unfortunately, no experimental data are available for K^+:CN^- or similar pair defects in cesium halide matrices. However, a rough estimate can be gained by a comparison with unpaired CN^- defects. Field and Sherman have measured a frequency shift of $\sim 0.6\ \mathrm{cm}^{-1}$/kbar for the fundamental ν_0 transition of substitutional CN^- in CsCl at 90 K.[39] With a corresponding shift of $\sim 1.2\ \mathrm{cm}^{-1}$/kbar for the second harmonic transition, Eq. (C2) yields $\Delta\lambda_1 \approx 3\times 10^{-3}$. If we assume the same $\Delta\lambda_1$ for a K^+:CN^- pair defect, we can then estimate the coupling tensor $\overleftrightarrow{D}$ to

$$\mathrm{D} \approx 3\times 10^{-3}\begin{bmatrix} 1 & 0 & 0 \\ 0 & 0 & 0 \\ 0 & 0 & 0 \end{bmatrix}\ . \tag{C3}$$

[1]For an overview see, e.g., *Persistent Spectral Hole-Burning: Science and Applications,* edited by W. E. Moerner (Springer, New York, 1988).

[2]M. Dubs and Hs. H. Günthard, Chem. Phys. Lett. **64**, 105 (1979); J. Mol. Struct. **60**, 311 (1980); M. Dubs, L. Ermanni, and Hs. H. Günthard, J. Mol. Spectrosc. **91**, 458 (1982).

[3]W. E. Moerner, A. R. Chraplyvy, and A. J. Sievers, Phys. Rev. B **29**, 6694 (1984).

[4]R. C. Spitzer, W. P. Ambrose, and A. J. Sievers, Phys. Rev. B **34**, 7307 (1986).

[5]S. P. Love, A. J. Sievers, B. L. Halfpap, and S. M. Lindsay, Phys. Rev. Lett. **65**, 1792 (1990).

[6]Y. Yang and F. Luty, Phys. Rev. Lett. **51**, 419 (1983).

[7]F. Rong, Y. Yang, and F. Luty, Cryst. Lattice Defects Amorphous Mater. **18**, 1 (1989).

[8]V. Dierolf and F. Luty, Rev. Solid State Science **4**, 479 (1990).

[9]W. Gellermann, Y. Yang, and F. Luty, Opt. Commun. **57**, 196 (1986); W. Gellermann and F. Luty, *ibid.* **72**, 214 (1989).

[10]W. D. Seward and V. Narayanamurti, Phys. Rev. **148**, 463 (1966).

[11]V. Narayanamurti and R. O. Pohl, Rev. Mod. Phys. **42**, 201 (1970).

[12]W. von der Osten and F. Luty, Phys. Rev. B **35**, 7684 (1987).

[13]M. Schrempel, W. Gellermann, and F. Luty, J. Lumin. **45**, 313 (1990).

[14]R. Nanz, Master's Thesis, University of Utah, 1985 (unpublished).

[15]L. Y. Chen, Master's Thesis, University of Utah, 1989 (unpublished).

[16]H. Adams, R. Brüggemann, P. Dietrich, D. Kirsten, H. Solka, and W. Urban, J. Opt. Soc. Am. B **2**, 815 (1985).

[17]J. Friedrich, D. Haarer, and R. Silbey, Chem. Phys. Lett. **95**, 119 (1983).

[18]D. Hsu and J. L. Skinner, J. Chem. Phys. **81**, 1604 (1984).

[19]D. Hsu and J. L. Skinner, J. Chem. Phys. **81**, 5471 (1984).

[20]D. Hsu and J. L. Skinner, J. Chem. Phys. **83**, 2097 (1985).

[21]D. Hsu and J. L. Skinner, J. Chem. Phys. **83**, 2107 (1985).

[22]D. Hsu and J. L. Skinner, J. Chem. Phys. **87**, 54 (1987).

[23]See, e.g., H. M. Sevian and J. L. Skinner, J. Chem. Phys. **91**, 1775 (1989) and references therein.

[24]With a coherent saturation experiment we measured $T_1=5$ ms at 5 K, $T_1=3$ ms at 25 K, and $T_1=1.5$ ms at 35 K for the second harmonic of the K^+:CN^- ν_2 transition in CsCl.

[25]E. Kröner, *Kontinuumstheorie der Versetzungen und Eigenspannungen* (Springer, New York, 1958); Arch. Ration. Math. Anal. **4**, 314 (1960).

[26]A. S. Nowick and W. R. Heller, Adv. Phys. **12**, 251 (1963).

[27]J. L. Black and B. I. Halperin, Phys. Rev. B **16**, 2879 (1977).

[28]L. D. Landau and E. M. Lifshitz, *Theory of Elasticity,* 3rd ed. (Pergamon, New York, 1986), Eqs. (22.1) and (22.6).

[29]R. T. Shuey and H. U. Beyeler, Z. Angew. Math. Phys. (Switzerland) **19**, 278 (1968).

[30]B. G. Dick, Phys. Rev. B **24**, 2127 (1981).

[31]D. Durand and F. Luty, Phys. Status Solidi B **81**, 443 (1977).

[32]S. R. Wilk and F. Luty, Phys. Status Solidi B **146**, 303 (1988).

[33]A. A. Z. Ahmad, H. G. Smith, N. Wakabayashi, and M. K. Wilkinson, Phys. Rev. B **6**, 3956 (1972).

[34]A. S. Barker, Jr. and A. J. Sievers, Rev. Mod. Phys. **47**, suppl. 2 (1975).

[35]S. R. Wilk, Dissertation, University of Utah, 1987 (unpublished).

[36]G. Simmons and H. Wang, *Single Crystal Elastic Constants and Calculated Aggregate Properties: A Handbook,* 2nd ed. (M.I.T. Press, Cambridge, Massachusetts, 1971).

[37]F. Luty, Phys. Rev. B **10**, 3677 (1974).

[38]H. U. Beyeler, Phys. Rev. B **11**, 3078 (1975).

[39]G. R. Field and W. F. Sherman, J. Chem. Phys. **47**, 2378 (1967).

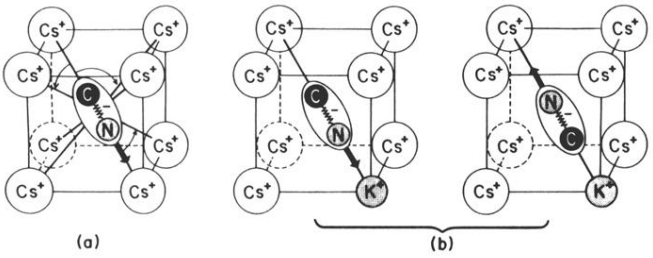

FIG. 1. Schematic illustration of ionic structure of CN^- defects in cesium halides. (a) Isolated CN^- defect: weakly hindered rotor between eight equivalent $\langle 111 \rangle$ orientations; (b) CN^- defect aligned in two opposite $\langle 111 \rangle$ electric dipole orientations by neighboring K^+ impurity.